metals

MDPI

Article

Modelling Crack Growth in Additively Manufactured Inconel 718 and Inconel 625

Rhys Jones [1,2,*], Andrew Ang [1], Daren Peng [1,2], Victor K. Champagne [3], Alex Michelson [4] and Aaron Birt [4]

[1] ARC Industrial Transformation Training Centre on Surface Engineering for Advanced Materials, School of Engineering, Swinburne University of Technology, John Street, Hawthorn, VIC 3122, Australia; aang@swin.edu.au (A.A.)
[2] Centre of Expertise for Structural Mechanics, Department of Mechanical and Aerospace Engineering, Monash University, Clayton, VIC 3800, Australia
[3] US Army Research Laboratory, U.S. Army Combat Capabilities Development Command Weapons and Materials Research Directorate, Aberdeen Proving Ground, Adelphi, MD 20783-1138, USA
[4] Solvus Global, 104 Prescott Street, Worcester, MA 01605, USA
* Correspondence: rhys.jones@monash.edu

Abstract: This paper first examines crack growth in a range of tests on additively manufactured (AM) and conventionally manufactured Inconel 718. It is shown that whereas when the crack growth rate (da/dN) is plotted as a function of the range of the stress intensity factor (ΔK), the crack growth curves exhibit considerable scatter/variability, when da/dN is expressed in terms of the Schwalbe crack driving force ($\Delta\kappa$), then each of the 33 different curves essentially collapse onto a single curve. This relationship appears to hold over approximately six orders of magnitude in da/dN. The same phenomenon also appears to hold for 20 room temperature tests on both conventionally and additively manufactured Inconel 625. Given that the 53 studies examined in this paper were taken from a wide cross section of research studies it would appear that the variability in the da/dN and ΔK curves can (to a first approximation) be accounted for by allowing for the variability in the fatigue threshold and the cyclic fracture toughness terms in the Schwalbe crack driving force. As such, the materials science community is challenged to address the fundamental science underpinning this observation.

Keywords: additive manufacturing; Inconel 718; Inconel 625; crack growth; Nasgro

Citation: Jones, R.; Ang, A.; Peng, D.; Champagne, V.K.; Michelson, A.; Birt, A. Modelling Crack Growth in Additively Manufactured Inconel 718 and Inconel 625. *Metals* **2023**, *13*, 1300. https://doi.org/10.3390/met13071300

Academic Editor: Petru Berce

Received: 21 June 2023
Revised: 16 July 2023
Accepted: 17 July 2023
Published: 20 July 2023

1. Introduction

Durability and damage tolerance (DADT) analyses are essential for the design and through-life sustainment of both aircraft and reusable space vehicles, as described in the United States Air Force (USAF) MIL-STD-1530D [1], United States (US) Joint Services Structural Integrity Guidelines JSSG2006 [2], and National Aeronautics and Space Administration (NASA) NASA-HDBK-5010 [3]. Furthermore, as delineated in USAF Structures Bulletin EZ-19-01 [4] a damage tolerance and durability-based approach is also mandated for the airworthiness certification of additively manufactured airframes and limited life aerospace parts. Indeed, MIL-STD-1530D [1] mandates that these analyses must be based on linear elastic fracture mechanics. At this stage, it should be noted that USAF Structures Bulletin EZ-19-01 [4] states that the most difficult challenge is to establish an accurate fracture mechanics-based prediction of structural performance and that, as highlighted in the United States Joint Services Structural Integrity Guidelines JSSG2006 [2], there must be no yielding at 115% design limit load, where the design limit load is the maximum load that will be seen in an operational airframe. Furthermore, as first outlined in [5] and discussed in more detail in [6–8], the mandated durability analysis must use the small crack growth curve and must be consistent with the building block approach mandated in MIL-STD-1530D and discussed in JSSG2006. This latter statement means that the same crack growth equation used to describe the growth of small cracks in laboratory test specimens must be

able to predict small crack growth under operation flight loads. In other words, there can be no disposable constants that are used to fit the measured experimental/operational crack growth history. As such, the equation governing the growth of small naturally occurring cracks in AM materials becomes particularly significant. The ASTM E647-13a [9] definition of small and short cracks is given in Appendix A.

In this context, it is now known that the Hartman–Schijve variant of the Nasgro crack growth equation can often be used to represent the growth of both long and short cracks in AM materials [7,8,10–23], cold spray additively manufactured (CSAM) parts [8,24,25], and to compute the durability of cold spray repairs to conventionally built aluminium alloys parts [26].

Important features of this formulation are that it has been shown [7,8,10–26] to:

(1) Account for the effect of the build direction on crack growth;
(2) Account for the large scatter seen in the da/dN versus ΔK curves associated with different AM processes;
(3) Be able to capture the growth of both long and small cracks in AM parts;
(4) Be able to predict the growth of cracks that arise due to the interaction between rough surfaces and surface breaking cracks;
(5) Be able to predict the growth of cracks that nucleate and grow from surface breaking porosity;
(6) Be able to compute the growth of cracks in cold spray repairs to corrosion damage.

Applications of this formulation to a range of conventionally manufactured materials are given in [6,27–33]. Its applicability to model crack growth in polymers, adhesives, composites, and nano-composites is discussed in [8,34–46]. An illustration of its ability to model crack growth in plasma sprayed refractory materials is given in [47].

The Hartman–Schijve crack growth equation can be expressed [7] as:

$$da/dN = D[\Delta\kappa]^p \tag{1}$$

where N is the number of cycles, a is the crack length/depth, p and D are material constants, and $\Delta\kappa$ is Schwalbe's crack tip driving force [48], viz:

$$\Delta\kappa = [(\Delta K - \Delta K_{thr})/(\sqrt{}(1 - K_{max}/A))] \tag{2}$$

Here, K_{max} and K_{min} are the maximum and minimum values of stress intensity factors in a given fatigue cycle, $\Delta K = (K_{max} - K_{min})$, ΔK_{thr} is the fatigue threshold, which is defined such that when $\Delta K = \Delta K_{thr}$, the crack growth rate (da/dN) becomes identically zero, and A is the cyclic fracture toughness. As explained in [6–8], the terms ΔK_{thr} and A are best interpreted as parameters that are chosen so as to fit the measured da/dN versus ΔK data. (A summary of alternative equations that are commonly used to compute the growth of long cracks is given in [49]).

An intriguing feature of this formulation is that it is now known [8] that the variability in the da/dN versus ΔK curves associated with AM Ti-6Al-4V is captured by allowing for the variability in the two parameters ΔK_{thr} and A, and that D and p would appear to be true material parameters. By this, it is meant that for AM Ti-6Al-4V, the parameters D and p would appear to be independent of the build process and the orientation of the crack to the build direction. As such, this discovery simplifies our understanding of the key parameters governing crack growth in AM Ti-6Al-4V. As a result, when da/dN is plotted against $\Delta\kappa$ the 53 curves, which were obtained by a number of independent researchers, it essentially fell onto a single curve [8]. Furthermore, as discussed in [8], since there are only two variable parameters, namely ΔK_{thr} and A, this means that the worst case (mean-3σ, where is the variance) da/dN versus ΔK curve, that is mandated in NASA-HDBK-5010, can be easily determined. As such the purpose of the present paper is to address the question: Does this phenomenon also hold for both Inconel 718 and Inconel 625?

For the sake of comparison, Table 1 presents the values of p and D associated with several AM materials.

Table 1. Values of p and D associated with a number of AM materials, data from refs [16–18].

Material and Reference	D	p
Ti-6Al-4V, from [16,18]	2.79×10^{-10}	2.12
316L Stainless Steel, from [16,25]	1.49×10^{-10}	2.12
AerMet 100, from [16]	1.49×10^{-10}	2.12
Inconel 625, from [17]	2.79×10^{-10}	1.99
17-4 PH Stainless Steel, from [17]	4.46×10^{-10}	1.83

2. Materials and Methods

Progress in science involves the interplay between theory and observation. In this context, it has been mentioned that for AM Ti-6Al-4V, it would appear that the variability in the long crack da/dN versus ΔK curves is essentially controlled by just two material parameters, namely ΔK_{thr} and A. The question thus arises: Is this true for other AM materials.

To address this question, it is necessary to focus on materials for which there are sufficient crack growth data to enable a reasonable conclusion to be reached. As a result, this paper studies crack growth in:

(i) Thirty-three tests on both conventionally built and AM Inconel 718 specimen tests, including the NASA round robin study into additively manufactured Inconel 718 built using selective laser melt (SLM) [50].
(ii) Twenty tests on both AM and conventionally built Inconel 625.

In each case, the crack growth data were taken from the open literature, and the da/dN versus ΔK curves were determined as per the ASTM E647 fatigue test standard [9]. In contrast, for these materials, the parameters D and p would appear to be true material constants.

This study reveals that, to a first approximation, the variability in the da/dN versus ΔK curves associated with each of the materials examined can be approximated using Equations (1) and (2) and allowing for the variability in the terms ΔK_{thr} and A. This finding simplifies our understanding of the role of the various terms in the Hartman–Schijve crack growth equation.

Given that this finding mirrors that for AM Ti-6Al-4V and for a range of other AM materials [16–18], as well as for a range of cold spray additively manufactured materials [24,25], the materials science community is challenged to address the fundamental science underpinning this observation.

We have previously explained that durability analysis is the key to the airworthiness certification of limited life AM parts, and that such analyses need to use the associated worst case small crack da/dN versus ΔK curve. In this context, [8] notes that this worst-case curve can often be estimated from the long crack curve by setting the fatigue threshold term in Equation (2) to a small value typically in the range $0.1 \leq \Delta K_{thr} \leq 0.3$. This suggestion is supported by the results given in [14,15,19,21,24] for the growth of small cracks in a range of AM materials. Unfortunately, a detailed search of the open literature did not reveal the necessary small crack da/dN versus ΔK curves for either Inconel 718 or Inconel 625. As a result, the methodology delineated in [8] is used to hypothesise the necessary worst-case curves. In so doing, this paper presents a means for these predictions to be independently (and scientifically) validated by researchers in the field. However, it should be noted that, as illustrated in [18], researchers should be aware of the need to determine sufficient crack growth curves that the variability in the curves can be adequately captured and the worst possible crack growth curve determined.

3. Crack Growth in Conventionally and Additively Manufactured Inconel 718

The NASA Round Robin study into crack growth in Selective Laser Melt (SLM) built Inconel 718 [50] presented both the $R = 0.1$ and the $R = 0.7$ da/dN versus ΔK curves. These curves, which were obtained by a number of laboratories, are shown in Figures 1–3. The

identifiers used in Figures 1–3 and Table 2 to identify the various laboratories that took part in this study are those used in [50]. Figures 1–3 also include the following da/dN versus ΔK curves:

(1) The room temperature R = 0.1, 0.4, 0.7, and 0.8 crack growth curves given in the Nasgro database. The Specimen ID's (descriptors) used for these tests in the Nasgro database are: Q3LA12AB01A4, Q3LA12AB01A3, Q3LA12AB01A2, and Q3LA12AB01A1, respectively.
(2) The R = 0.1 crack growth curve given by Konecna et al. [51] for SLM Inconel 718;
(3) The R = 0.1 and 0.7 crack growth curves given by Newman and Yamada [52] for conventionally manufactured Inconel 718;
(4) The R = 0.1 and 0.7 crack growth curves given by Yadollahi et al. [53] for laser bed powder fusion (LPBF) built Inconel 718 specimens.
(5) The R = 0.1 and (high R ratio) K_{max} fatigue crack growth curves given by Ostergaard et al. [54] for LPBF Inconel 718. These curves are for specimens both with and without HIPing. Following the notation used in [54], specimens that were subjected to both solution and duplex aging are given the suffix S-DA. Specimens that have been HIPed include the term HIP in their descriptor. Details of these two post-build treatments are given in [54].
(6) The R = 0.1 crack growth curve given by Kim et al. [55] for LPBF Inconel 718;
(7) The R = 0.1 crack growth curve given by Yu et al. [56] for laser-directed energy deposition (LDED) built Inconel 718 in the as-deposited condition.
(8) The R = 0.5, 0.1, −1.0, and −2 crack growth curves given by Paluskiewicz et al. [57] for conventionally manufactured Inconel 718 tested at 100 °C.

An interesting feature of Figure 2 is the large variability in the R = 0.1 da/dN versus ΔK curves at low values of da/dN and the relatively low variability at higher values of da/dN.

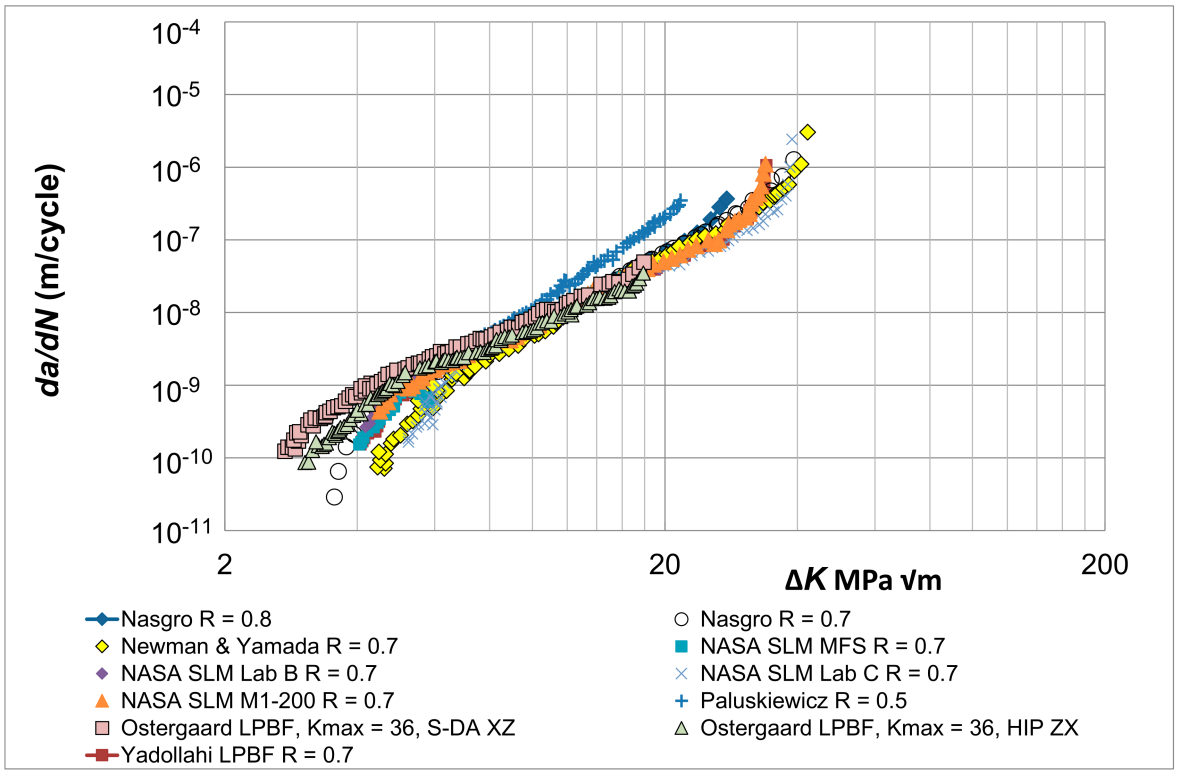

Figure 1. The high R ratio da/dN versus ΔK curves for tests on both conventionally manufactured and AM Inconel 718. Here it should be noted that the curves with the prefix "NASA SLM" are data from ref. [50].

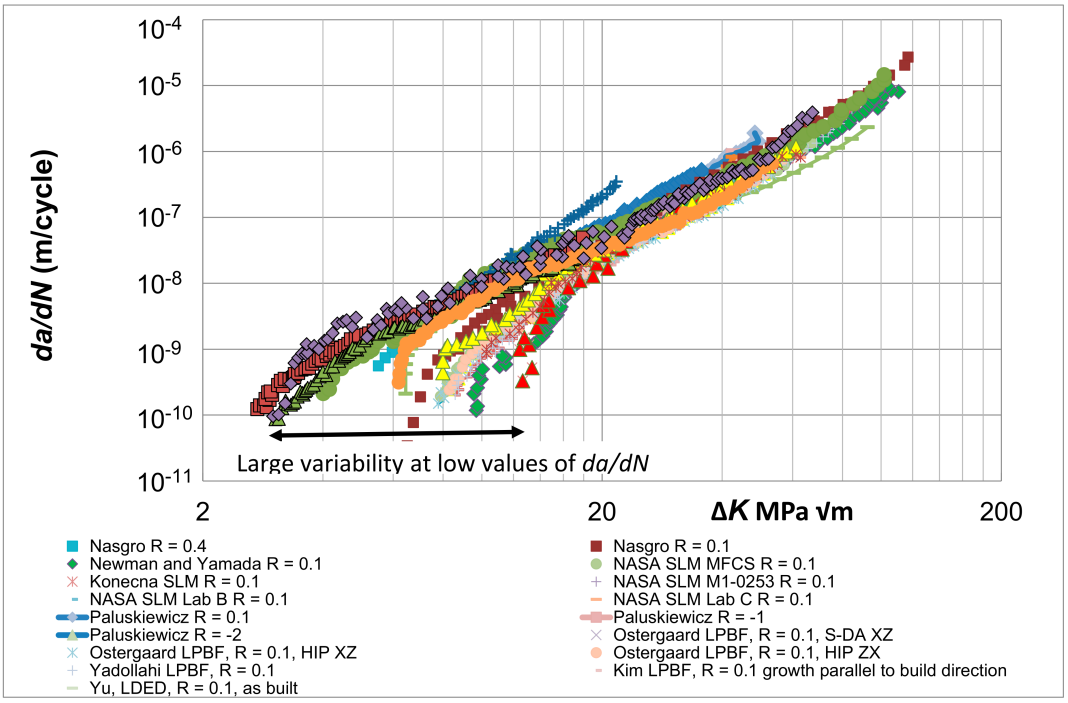

Figure 2. The R = 0.1 and 0.4 da/dN versus ΔK curves for tests on conventionally manufactured Inconel 718 and the various R = 0.1 and 0.4 da/dN versus ΔK curves for AM Inconel 718 together with the curves given by Paluskiewicz [58] for conventionally manufactured Inconel 718 tested at 100 °C and at a range of R ratios. As per Figure 1, curves with the prefix "NASA SLM" are data from ref. [50].

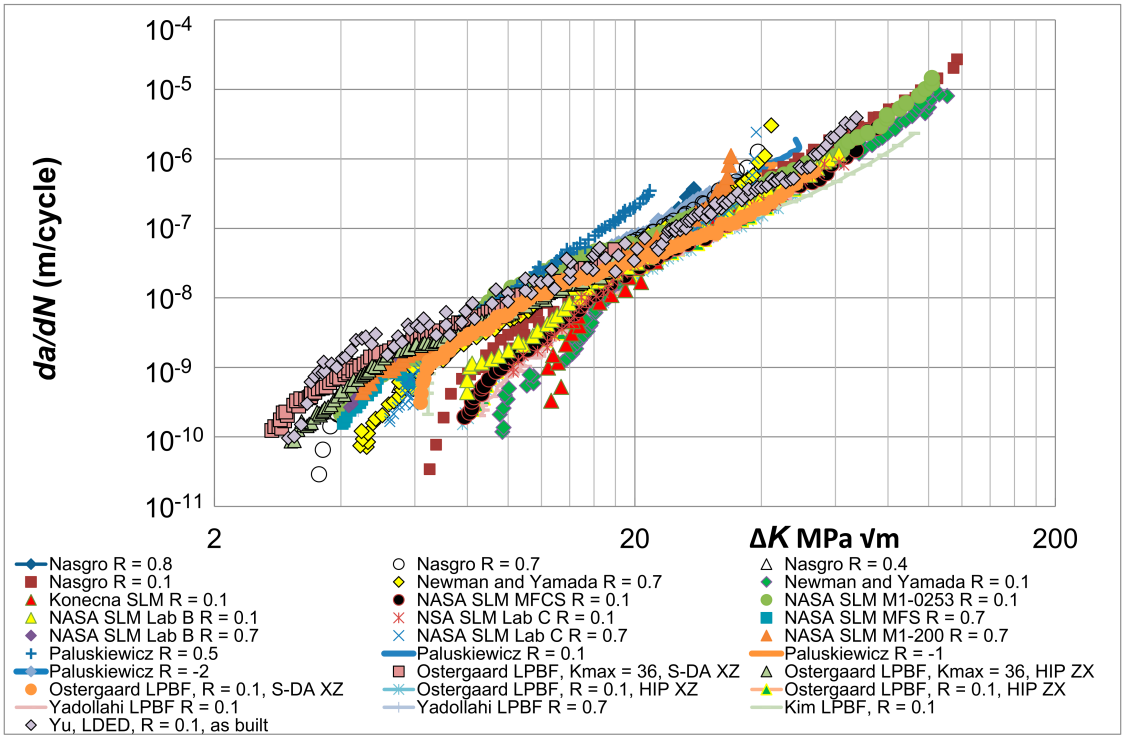

Figure 3. A combined plot of the 28 da/dN versus ΔK curves shown in Figures 1 and 2. This plot covers a range of build processes and R ratios.

Low Temperature Crack Growth in Conventionally Manufactured Inconel 718

Since Inconel 718 is also widely used in space-related applications, let us next consider the effect of low temperatures on the da/dN versus ΔK curves associated with conventionally manufactured Inconel 718. To this end, Figure 4 presents a few selected da/dN versus ΔK curves taken from Figure 3 together with the following datasets that were extracted from the Nasgro database, viz:

(1) Specimen test ID: Q3LB11AA07A2. This is a middle crack tension (M(T)) specimen cut from a 12.7 mm thick sheet and tested at R = 0.6 and 195 °K.
(2) Specimen test ID: Q3LB11AA07A1. This is a middle crack tension specimen (M(T)) cut from a 12.7 mm thick sheet and tested at R = 0.33 and 195 °K.
(3) Specimen test ID: Q3LB24GB04A1. This is a 25.4 mm thick compact tension (CT) specimen cut from a forging and tested at R = 0.1 and 76 °K.
(4) Specimen test ID: Q3LC10LA04A1. This is a 7.62 mm thick compact tension (CT) specimen cut from a plate and tested at R = 0.1 and 77.6 °K.
(5) Specimen test ID: Q3LB24GC02A1. This is a 25.4 mm thick compact tension (CT) specimen cut from a forging and tested at R = 0.1 and 4 °K.

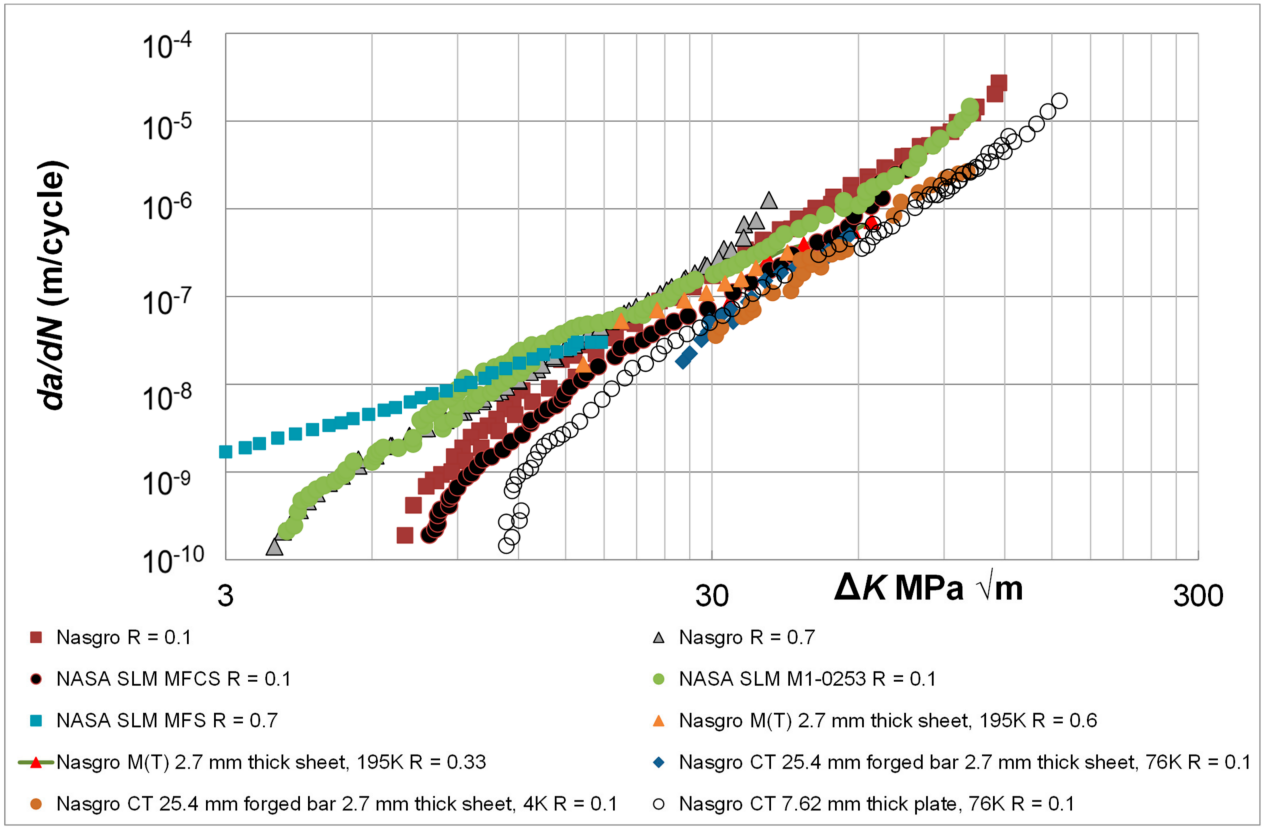

Figure 4. The da/dN versus ΔK relationship obtained tests performed at 4 °K, 76 °K, and 195 °K together a few selected curves shown in Figure 3.

Examining Figure 4, we see that, to a first approximation, low temperatures appear to improve the fatigue performance of Inconel 718.

Having presented a range of da/dN versus ΔK crack growth curves associated both conventionally manufactured and AM Inconel 718, the next section examines the question:

Do these curves simplify if da/dN is expressed as a function of $\Delta\kappa$, and can, as has been shown [8] to be the case for AM Ti-6Al-4V, the variability in the da/dN versus ΔK curves be captured by allowing for the variability in the two parameters ΔK_{thr} and A?

4. Modelling the Variability in Crack Growth in Conventionally Manufactured Inconel 718 and Additively Manufactured Inconel 718

Figure 5 reveals that, to a first approximation, when da/dN is plotted against $\Delta\kappa$ then the various (28) curves shown in Figure 3, that cover both conventionally built and AM Inconel 718 tested at a range of R ratios, all (essentially) collapse onto a single master curve, viz:

$$da/dN = 1.2 \times 10^{-10} \times [\Delta\kappa]^{2.12} \quad (3)$$

The values of the parameters ΔK_{thr} and A used in Figure 5, which were determined using the "Automated Total Least Squares" methodology described in [58], are listed in Table 2. Furthermore, as can be seen in Figure 5, this da/dN versus $\Delta\kappa$ relationship appears to hold over approximately six orders of magnitude in da/dN, and holds regardless of whether the material was fabricated conventionally, using SLM, L-PBF, or LDED. It also appears to hold regardless of the R ratio. We also see that for SLM, L-PBF, and LDED Inconel 718, the value of the exponent p in Equation (1) is approximately 2, and hence is similar to the values obtained for the AM materials listed in Table 1. Interestingly, examining Figure 5, we see that the da/dN versus $\Delta\kappa$ curve associated with SLM, L-PBF, and LDED built Inconel 718 is similar to the da/dN versus $\Delta\kappa$ curves associated with additively manufactured Ti-6Al-4V, 17-4Ph steel, and Inconel 625.

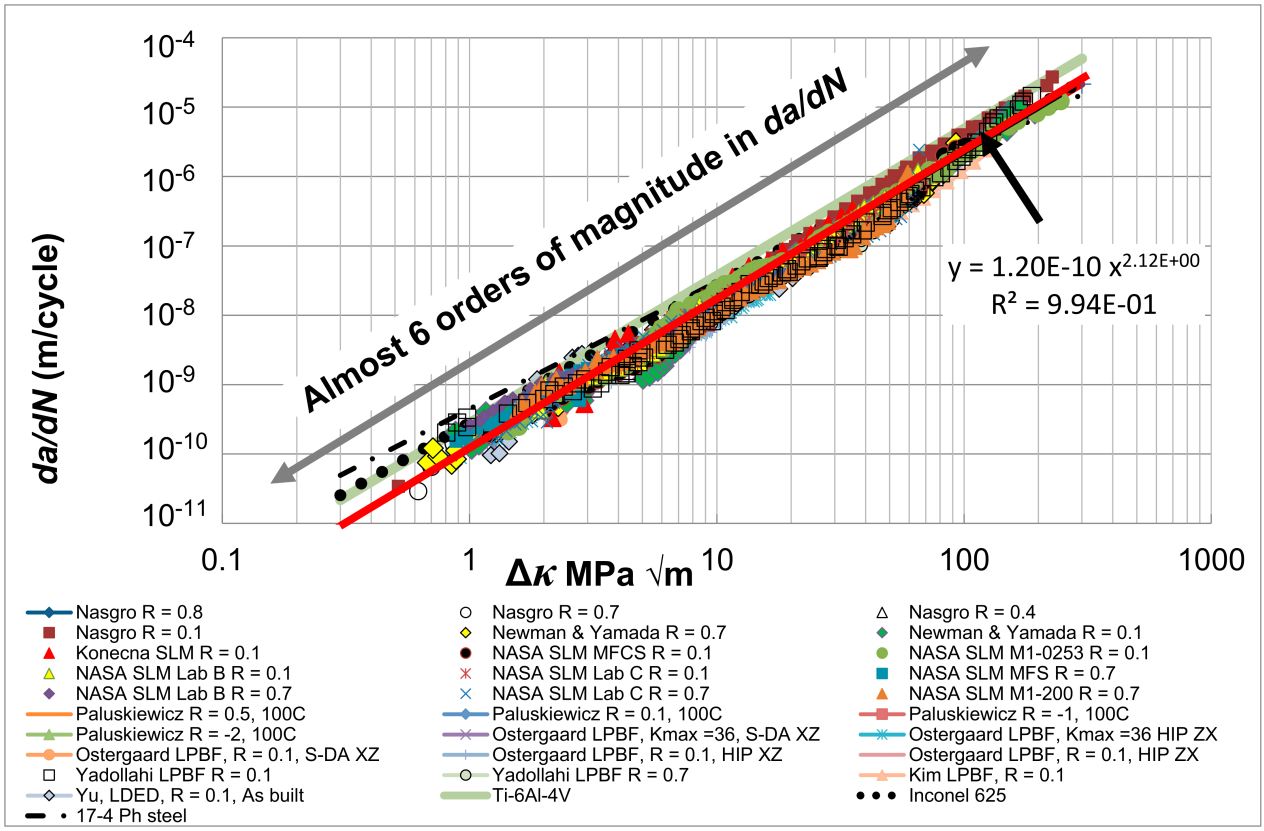

Figure 5. The da/dN versus $\Delta\kappa$ relationship obtained for all of the 33 datasets shown in Figures 1–4.

Table 2. Values of the parameters used in Figures 5 and 6.

Test Descriptor [1]	ΔK_{thr} (MPa $\sqrt{m}$)	A (MPa $\sqrt{m}$)	Coefficient of Determination (R^2)
$R = 0.1$			
[++] NASA SLM M1-0253 * [50]	2.6	160	0.85
NASA SLM MFSC [50]	6.2	155	0.83

Table 2. *Cont.*

Test Descriptor [1]	ΔK_{thr} (MPa $\sqrt{m}$)	A (MPa $\sqrt{m}$)	Coefficient of Determination (R^2)
NASA SLM Lab B [50]	6.1	240	0.81
NASA SLM Lab C [50]	7.8	180	0.99
Nasgro data base, room temperature test, Nasgro specimen ID: Q3LA12AB01A4	6.0	170	
Konecna et al. [51]	1.8	140	
Yadollahi et al. [53] (L-PBF)	7.8	150	
Newman et al. [52], conventionally manufactured	8.7	175	
Kim et al. [55] for LPBF	4.0	180	
Yu et al. [56] LED tested in the as-built condition	1.8	118	
$R = 0.4$			
Nasgro data base, room temperature test, Specimen ID: Q3LA12AB01A3	3.5	170	
$R = 0.7$			
NASA SLM M1-200 [50]	3.0	155	0.80
NASA SLM MFSC [50]	3.0	155	0.83
NASA SLM Lab B [50]	2.9	240	0.90
NASA SLM Lab C [50]	4.1	180	0.80
Newman et al. [52], conventionally manufactured	3.0	175	
Nasgro data base, room temperature test, Nasgro specimen ID: Q3LA12AB01A2	2.95	170	
Yadollahi et al. [53] (L-PBF)	3.0	150	
Yu et al. [55] LED tested in the as-built condition	1.8	118	
Nasgro data base $R = 0.8$, room temperature test, Nasgro specimen ID Q3LA12AB01A1	4.0	170	
Paluskiewicz et al. [57], conventionally built Inconel 718 tested at 100 °C (373 °K) at a range of R ratios			
$R = 0.5$	2.0	70 **	
$R = 0.1$	6.0	70	
$R = -1.0$	9.0	70	
$R = -2.0$	4.0	70	
Ostergaard et al. [56], LPBF built Inconel 718			
$K_{max} = 36$ MPa $\sqrt{m}$, SD-A with the crack in the XZ direction	1.8	150	
$K_{max} = 36$ MPa $\sqrt{m}$, HIP with the crack in the ZX direction	2.3	150	
$R = 0.1$, SD-A with the crack in the XZ direction	3.9	150	
$R = 0.1$, HIP with the crack in the XZ direction	6.7	150	
$R = 0.1$, HIP with the crack in the ZX direction	7.0	150	
Nasgro Low temperature tests on conventionally built Inconel 718			

Table 2. *Cont.*

Test Descriptor [1]	ΔK_{thr} (MPa $\sqrt{m}$)	A (MPa $\sqrt{m}$)	Coefficient of Determination (R^2)
12.7 mm thick M(T) specimen tested at R = 0.6 and 195 °K, Nasgro Specimen ID: Q3LB11AA07A2.	7.0	250	
12.7 mm thick M(T) specimen tested at R = 0.33 and 195 °K, Nasgro specimen ID: Q3LB11AA07A2.	13.0	250	
25.4 mm thick CT specimen tested at R = 0.1 and 76 °K, Nasgro specimen test ID: Q3LB24GB04A1.	17	140	
7.62 mm thick CT specimen tested at R = 0.1 and 76 °K, Nasgro specimen test ID: Q3LC10LA04A1.	3.9	150	
25.4 mm thick CT specimen tested at R = 0.1 and 4 °K, Nasgro specimen test ID: Q3LB24GC02A1.	18	200	

[1] Unless stated the specimen tests were compact tension (CT) specimens and the tests were performed in accordance with the fatigue test standard ASTM E647-13a. * Unless stated the specimens were tested at room temperature. ** These test specimens would appear to have a reduced value of A. It is not clear why this is the case. [++] The prefix "NASA SLM" denotes data from the NASA round robin study into crack growth in Inconel 718 [50].

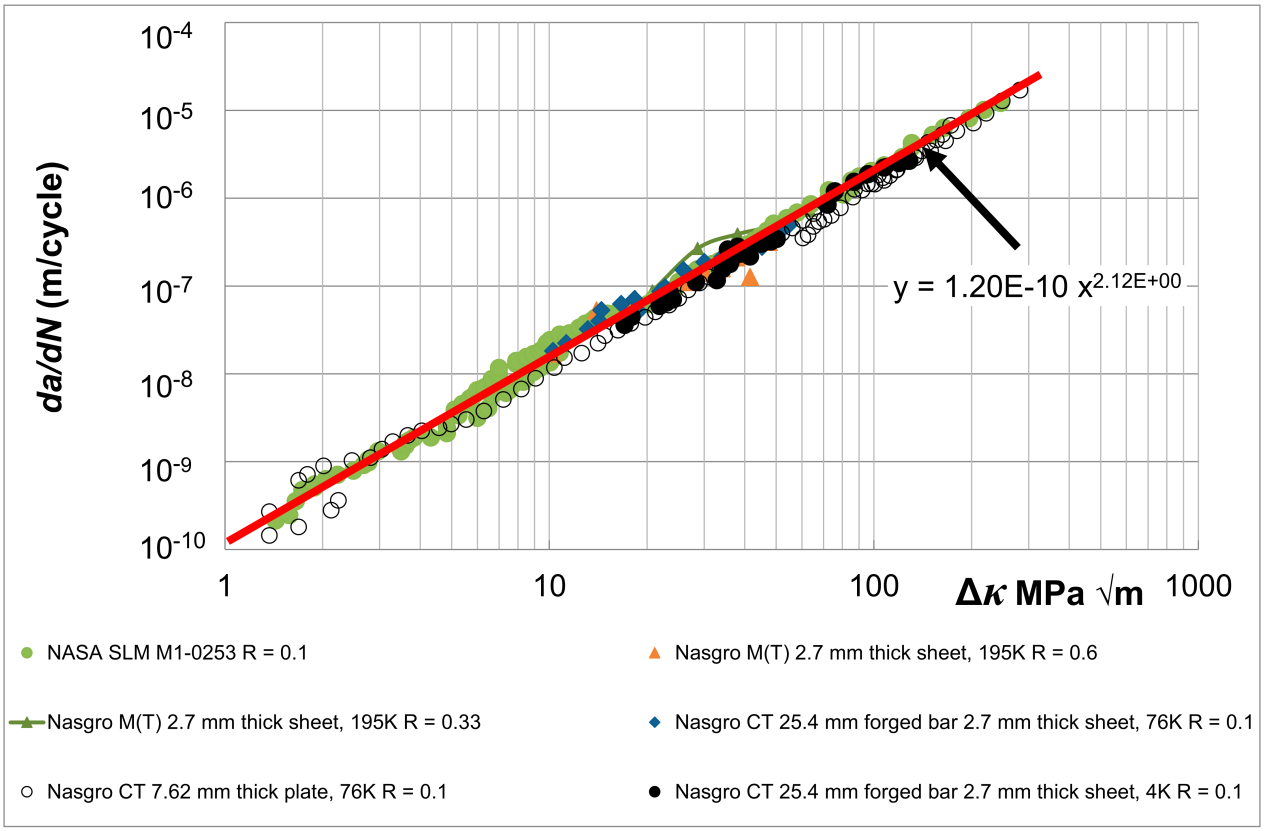

Figure 6. The da/dN versus $\Delta\kappa$ relationship associated with tests performed at a range of low temperatures together with the master curve representation shown in Figure 5, i.e., Equation (3).

Figure 6 reveals that, for the low temperature curves shown in Figure 4, when da/dN is plotted against $\Delta\kappa$, these curves also collapse onto Equation (3). The values of the parameters ΔK_{thr} and A used in Figure 6 are also listed in Table 2. Consequently, not only do these curves simplify if da/dN is expressed as a function of $\Delta\kappa$, but (to a first approximation) the variability in the curves can be captured by allowing for the variability

in the two parameters ΔK_{thr} and A. To compliment Figure 6, Appendix B presents a selection of cases where the measured and computed da/dN is plotted against ΔK curves are compared. The computed da/dN is plotted against ΔK curves obtained using Equation (3) and the values of ΔK_{thr} and A listed in Table 2.

5. Modelling the Variability in Crack Growth in Conventionally Manufactured and Additively Manufactured Inconel 625

Section 3 noted that the da/dN versus $\Delta\kappa$ relationship determined in [14] for a limited number of tests on AM Inconel 625 was similar to that of Inconel 718. Let us further investigate this observation by analysing the da/dN versus ΔK curves presented in [59–62] for tests on Inconel 625 specimens built using both SLM and LPBF where the cracks lay at various degrees to the build direction. Two SLM specimen tests were analysed in [59,62]. The R ratios in the tests discussed in [59] was 0.1. In Ref. [62], the SLM specimens were tested at R ratios of 0.1, 0.5, and 0.7. The SLM specimens in [59,62] were heat treated, but not HIPed. In Ref. [59], specimens with the crack in different directions, which were labelled SLM SR-0 or SLM-SR-90, were also tested. The SR notation indicates that the specimens were stress relieved, and the 0/90 notation indicates the direction of the crack relative to the build direction. The LPBF specimens tested in [60], at R ratios of 0.1, were either HIPed or stress relieved (SR). The LPBF specimens tested in [60] were assigned the designations P_0, P_1, P_2, and P_3 depending on the laser deposition parameters, [6] for details. In Ref. [60], tests were performed on specimens with the crack at either 0 and 90 degrees to the build direction The LBPF specimens tested in [61], which had an R ratio of 0.5, were labelled V2–V6 and tests were performed on specimens with the crack at 0 and 90 degrees to the build direction.

Figure 7 presents the R = 0.1 crack growth curves for both the AM specimens and the wrought material tested in [58]. Figure 8 presents the R = 0.5 and 0.7 curves given for this material. Figure 9 presents all of these curves on a single plot.

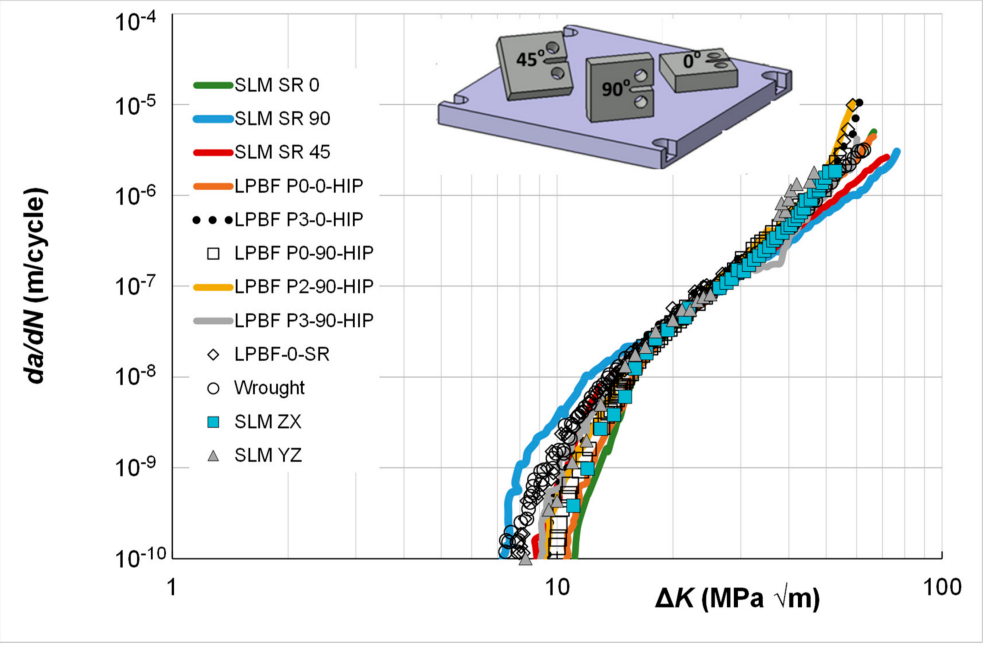

Figure 7. The twelve R = 0.1 da/dN versus ΔK curves for these various SLM and LPBF Inconel 625 tests with the crack at different angles to the build direction. Specimens labelled SLM SR are data from ref. [59], specimens labelled LPBF P_0 to P_3 are data from ref. [60]. Specimens labelled SLM ZX and SLM YZ are data from ref. [62]. The curve associated with the wrought material is data from ref. [59].

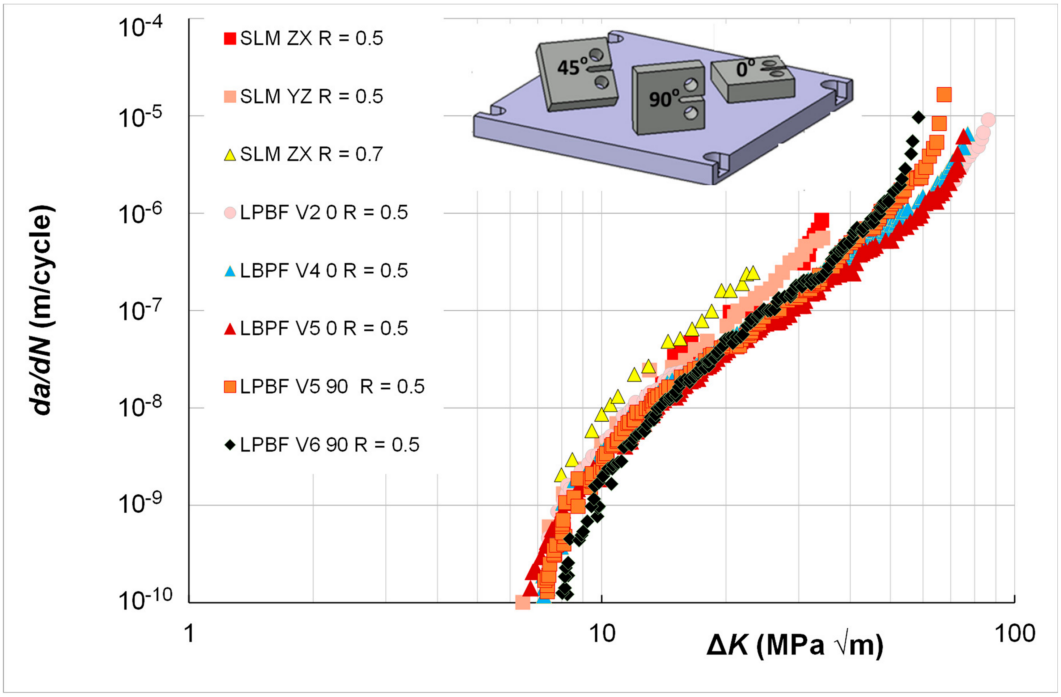

Figure 8. The eight da/dN versus ΔK curves for these various SLM and LPBF Inconel 625 tests at R ratios varying from 0.5 to 0.7 and with the crack at different angles to the build direction. Specimens labelled SLM SR are data from ref. [60], specimens labelled LPBF V2-V6 data from ref. [61], specimens labelled LPBF P_0 to P_3 are data from ref. [61]. Specimens labelled SLM ZX and SLM YZ are data from ref. [62].

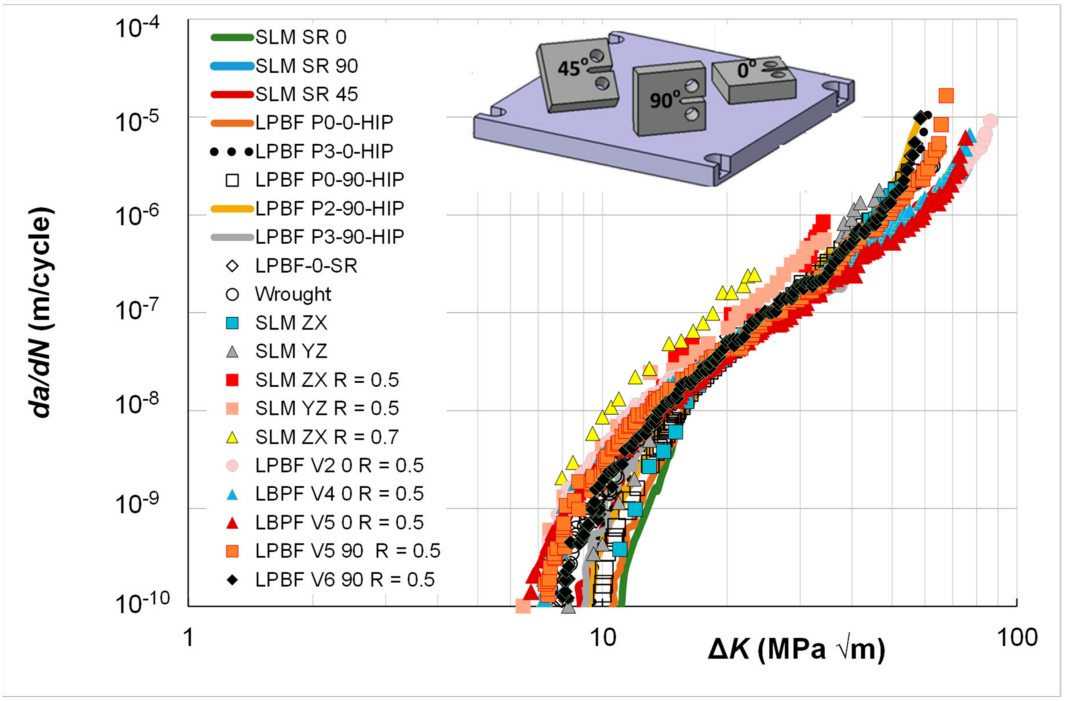

Figure 9. The 20 da/dN versus ΔK curves for these various SLM and LPBF Inconel 625 tests at R ratios varying from 0.1 to 0.7 and with the crack at different angles to the build direction. For those cases when the R ratio is not stated, then $R = 0.1$.

The resultant 20 different da/dN versus ΔK curves are given in Figure 9. The corresponding da/dN versus $\Delta\kappa$ curves are given in Figure 10 together with the governing equation published in a prior paper for this material [17], viz:

$$da/dN = 2.79 \times 10^{-10} (\Delta\kappa)^{1.99} \quad (4)$$

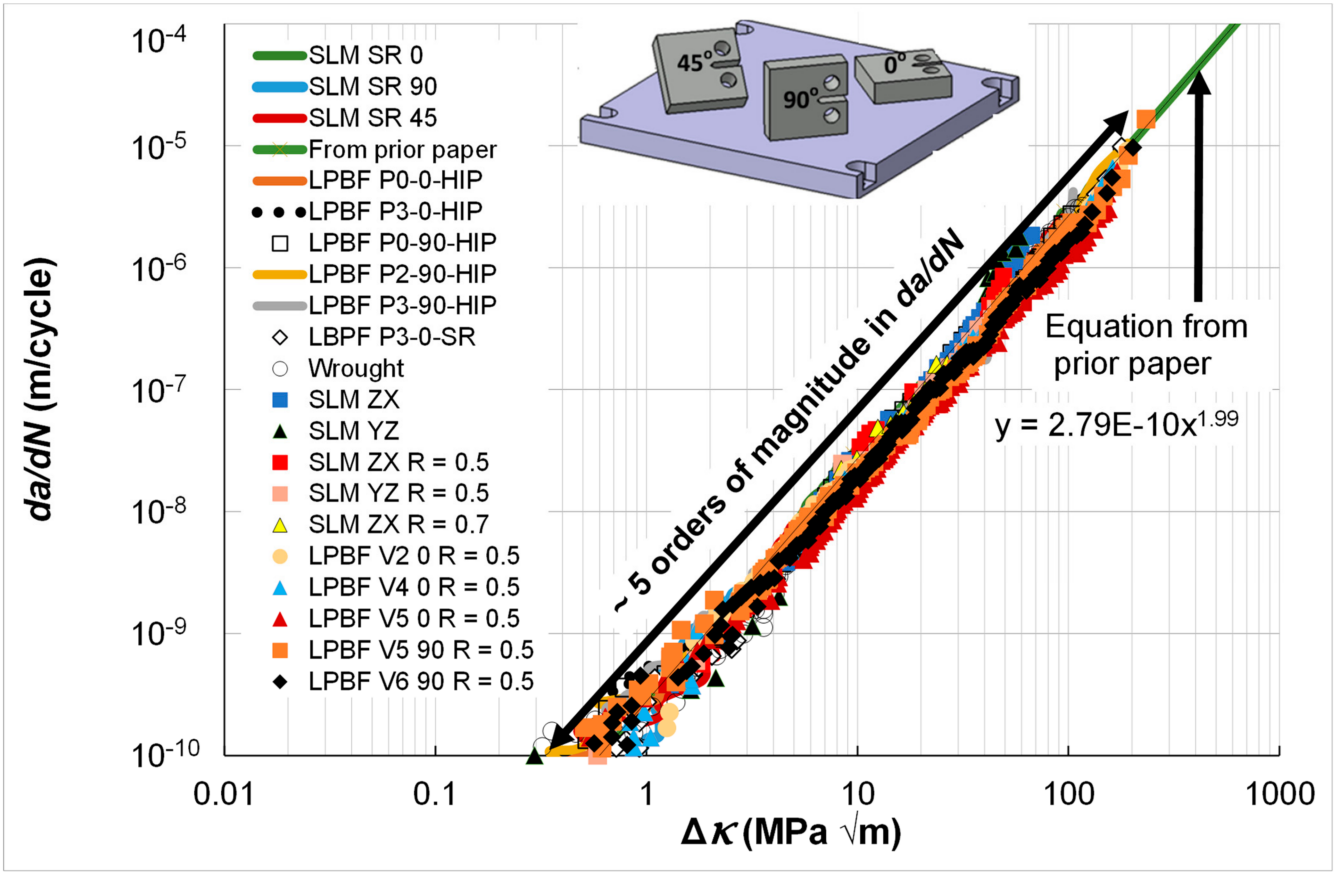

Figure 10. The da/dN versus $\Delta\kappa$ curves for the AM Inconel 625 tests shown in Figures 7–9.

Figure 10 reveals that, regardless of the AM process, the R ratio, or the angle between the crack and the build direction, when da/dN is plotted as a function of $\Delta\kappa$, then the 20 different curves essentially collapse onto a single master curve that can be approximated by Equation (4). As previously, the values of ΔK_{thr} and A used in Figure 10 were determined using the "Automated Total Least Squares" methodology described in [59]. The values of the parameters associated with these 20 tests are given in Table 3.

To compliment Figure 10, Appendix B presents a selection of cases where the measured and computed da/dN plotted against ΔK curves are compared. The computed da/dN plotted against ΔK curves are obtained using Equation (4) and the values of ΔK_{thr} and A listed in Table 3.

As such, this study supports the conclusion given above for crack growth in Inconel 718 and Ti-6Al-4V, namely that, to a first approximation, crack growth in these 20 tests would appear to be controlled by the two independent parameters A and ΔK_{thr}.

Table 3. Values of the parameters A and ΔK_{thr} used in Figure 10.

Test, Reference and Descriptor	ΔK_{thr} (MPa $\sqrt{m}$)	A (MPa $\sqrt{m}$)
SLM [59]		
SLM SR 0, R = 0.1	10.9	90
SLM SR 90, R = 0.1	6.4	140
SLM SR 45, R = 0.1	8.3	140
Wrought, R = 0.1	7.0	90
LPBF [60]		
LPBF P_0-0 HIP, R = 0.1	10.1	90
LPBF P_0-90 HIP, R = 0.1	9.5	76
LPBF P_2-90 HIP, R = 0.1	8.9	70
LPBF P_3-0 HIP, R = 0.1	8.8	74
LPBF P_3-90 HIP, R = 0.1	8.5	88
LPBF P_3-0 SR, R = 0.1	7.3	71
SLM [62]		
SLM ZX, R= 0.1	9.8	100
SLM YZ, R = 0.1	8.0	90
SLM ZX, R= 0.5	6.4	100
SLM YZ, R = 0.5	5.9	90
SLM ZX, R= 0.7	5.5	100
LPBF [61]		
LBPF V2 0, R = 0.5	6.2	210
LBPF V4 0, R = 0.5	6.4	190
LBPF V5 0, R = 0.5	6.2	180
LBPF V5 90, R = 0.5	6.7	145
LBPF V6 90, R = 0.5	7.4	125

6. The Small Crack Growth Hypothesis

Appendix X3 of the fatigue test standard ASTM E647-13a [9] comments: It is unclear if a measurable threshold exists for small naturally occurring cracks in operational structures. The papers [6,7,12,14,15,20,21,23,26,28–32,63] subsequently built on this statement to illustrate that, for both conventionally and AM metals, Equations (1) and (2) with the values of D, p, and A determined from tests on long cracks and the fatigue threshold set to a small value, typically in the range $0.1 \leq \Delta K_{thr} \leq 0.3$ MPa $\sqrt{m}$, were often able to accurately compute the growth of small cracks under both constant amplitude and operational flight loads.

As a result, it is hypothesised that, in the absence of significant residual stresses, an upper bound estimate of the growth of small cracks in Inconel 718, that is required by NASA-HDBK-5010, may be able to be estimated using Equation (3) with the fatigue threshold term ΔK_{thr} set to 0.1, viz:

$$da/dN = 1.2 \times 10^{-10} \times [(\Delta K - 0.1)/(\sqrt{(1 - K_{max}/A)})]^{2.12} \quad (5)$$

It is similarly hypothesised that, in the absence of significant residual stresses, an upper bound estimate of the growth of small cracks in Inconel 625 may be able to be estimated using Equation (4) with the fatigue threshold term ΔK_{thr} set to 0.1, viz:

$$da/dN = 2.79 \times 10^{-10} \times [(\Delta K - 0.1)/(\sqrt{(1 - K_{max}/A)})]^{1.99} \quad (6)$$

The values of A in Equations (5) and (6) would need to be taken from tests on long cracks in specimens built using the same processes and post build treatments as those used to build the small crack test specimens. However, it should be stressed that further work is needed to validate these hypotheses.

7. Conclusions

Whereas when da/dN is expressed as a function of the range of ΔK, the crack growth curves associated with 33 tests on both conventionally and additively manufactured Inconel 718 exhibit considerable scatter/variability, when da/dN is expressed in terms of $\Delta\kappa$, each of these 33 different curves essentially collapse onto a single curve regardless of the manufacturing process. Furthermore, to a first approximation, the resultant relationship between da/dN and $\Delta\kappa$ appears to hold over approximately six orders of magnitude in da/dN.

It would thus appear that accounting for the variability in the terms ΔK_{thr} and A in the Hartman–Schijve crack growth equation has the potential to account for both the variability in crack growth and the R ratio effect seen in crack growth tests on both AM and conventionally built Inconel 718. Furthermore, for tests on conventionally manufactured Inconel 718, this relationship appears to hold for tests performed at temperatures that range from 373 °K to cryogenic temperatures.

This finding suggests that since there are only two variable parameters, namely ΔK_{thr} and A, this formulation has the potential to determine the worst case (mean-3σ) da/dN versus ΔK curve mandated in NASA-HDBK-5010.

The same phenomenon also appears to hold for 20 room temperature tests on both conventionally and additively manufactured Inconel 625, albeit over approximately six orders of magnitude in da/dN.

We also found that the da/dN versus $\Delta\kappa$ curve associated with SLM, L-PBF, and LDED built Inconel 718 is similar to the da/dN versus $\Delta\kappa$ curves associated with additively manufactured Ti-6Al-4V, 17-4Ph steel and Inconel 625.

Unfortunately, the authors could not find a correlation between the values ΔK_{thr} and A determined in these studies and the corresponding build processes.

Furthermore, given that:

(1) the 53 studies examined in this paper were taken from a wide cross section of researchers;
(2) that the conclusions reached in this study mirror those stated in [8] for the assessment of 53 independent studies into crack growth in AM Ti-6Al-4V, which were also taken from a wide cross section of researchers, namely that the variability in the da/dN and ΔK curves can (to a first approximation) be accounted for by allowing for the variability in the terms ΔK_{thr} and A;
(3) the materials science community is challenged to address the fundamental science underpinning this observation.

Prior studies have shown how for AM Ti-6Al-4V, AM 316L stainless steel, and wire arc additively manufactured (WAAM) 18Ni 250 Maraging steel, the mandated worst case small crack da/dN versus ΔK curve can be obtained from a knowledge of the da/dN versus $\Delta\kappa$ curves by setting the term ΔK_{thr} to a small value (0.1 MPa $\sqrt{}$m). (To the best of the authors' knowledge, no other such predictive capability exists for AM materials.)

As a result, the present paper has, for the first time, taken the opportunity to predict the necessary worst case da/dN versus ΔK curves for both AM Inconel 718 and AM Inconel 625, and in the spirit of the scientific method, the materials science community is also challenged to measure these curves and thereby confirm or disprove these predictions.

The ability to predict the worst-case small crack da/dN versus ΔK curve for these two materials, when taken together with the prior studies mentioned above, would further support the generality of this approach and have the potential to significantly simplify the durability analysis/certification.

Author Contributions: Project overview in Australia, methodology, and the small crack hypothesis—R.J.; software development, implementation, and analysis—D.P.; funding procurement, data storage, supervision of D.P., and revision of the paper—A.A.; conceptualisation, programme overview, and corrections to paper—V.K.C., A.M. and A.B.; validation of analysis methodology—A.M.; first draft of the paper: R.J. and V.K.C. All authors have read and agreed to the published version of the manuscript.

Funding: Rhys Jones and Andrew Ang would like to acknowledge funding provided by the US Army International Technology Center, Indo-Pacific (ITC-IPAC), Tokyo, Contract No. FA520921P0164.

Data Availability Statement: The data are not yet publicly available due to the ongoing nature of this project. The data will be available on completion of the study.

Acknowledgments: The findings and conclusions or recommendations expressed in this paper are those of the authors and do not necessarily reflect the views of the ITC-IPAC.

Conflicts of Interest: The authors declare no conflict of interest.

Appendix A. The ASTM E647 Small and Short Crack Definitions

The ASTM E647-13a fatigue test standard [9] defines a crack as being small when all of the physical dimensions are small when compared to a physical size scale, continuum mechanics scale, or a relevant microstructural scale. For example, for a surface breaking crack to be small, both its depth and its surface crack length must meet these criteria. A crack is defined as short when only one physical dimension (for example, the length of a through-the-thickness crack) is small.

Appendix B. Computed and Measured Curves

To complement the da/dN versus $\Delta\kappa$ curves given in Figures 5, 6 and 10 for crack growth in Inconel 718 and Inconel 625, Figures A1–A3 present a selection of the predicted da/dN versus ΔK curves. (The option of plotting only a selection of curves was adopted due to the large number of curves analysed.) The computed curves shown in Figures A1 and A2 for Inconel 718 are obtained using Equation (3) and the values of ΔK_{thr} and A listed in Table 2. The computed curves shown in Figure A3 for Inconel 625 are obtained using Equation (4) and the values of ΔK_{thr} and A listed in Table 3.

These plots further illustrate the ability of Equations (1) and (2) with the values of ΔK_{thr} and A as given in Tables 1 and 2 to reasonably accurately represent crack growth in Inconel 718 and Inconel 625.

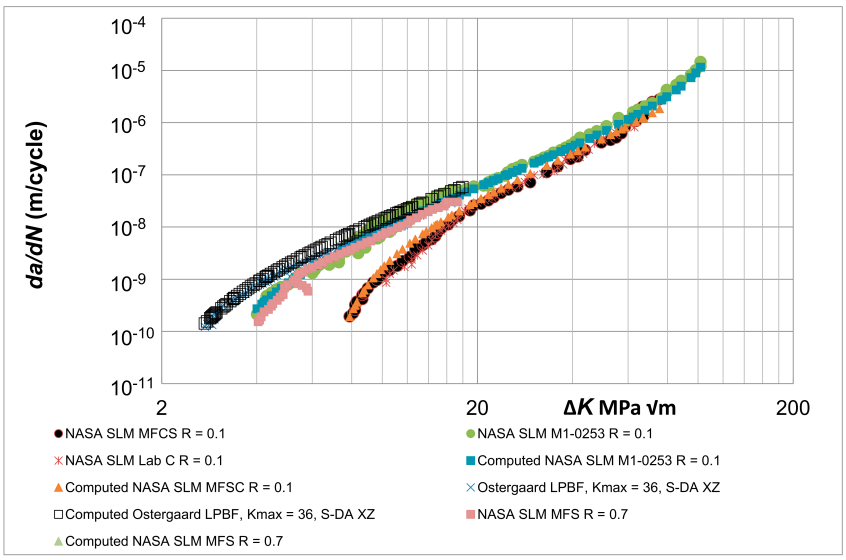

Figure A1. Comparison between selected computed and measured room temperature da/dN versus ΔK curves for AM Inconel 718.

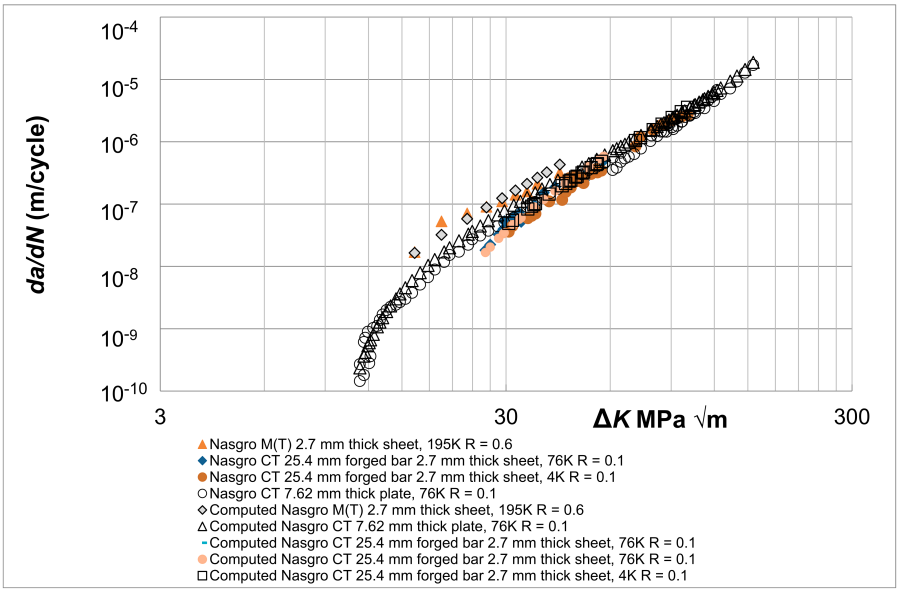

Figure A2. Comparison between selected computed and measured low temperature da/dN versus ΔK curves for AM Inconel 718.

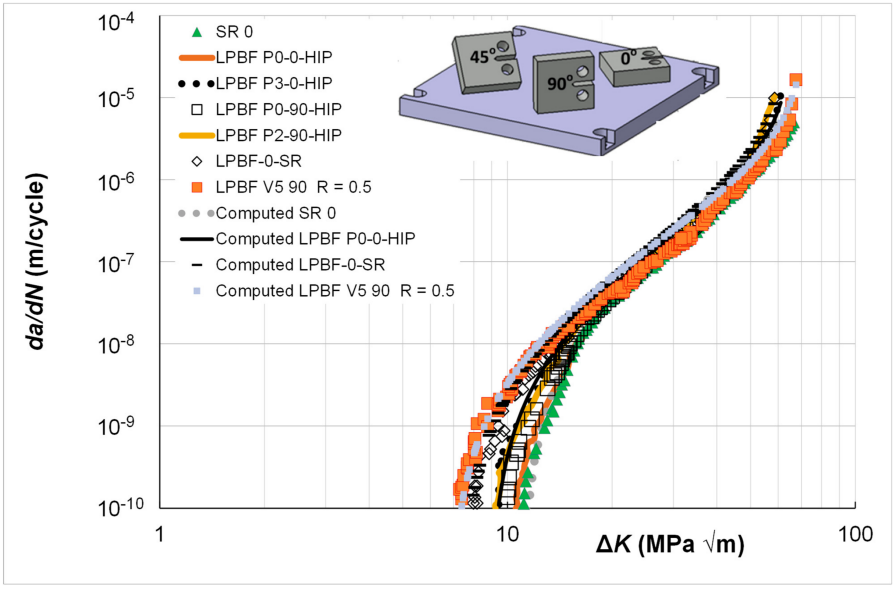

Figure A3. Comparison between selected computed and measured room temperature da/dN versus ΔK curves for AM Inconel 625.

References

1. *MIL-STD-1530D*; Standard Practice Aircraft Structural Integrity Program (ASIP). Department of Defense: Washington, DC, USA, 2016.
2. *JSSG-2006*; Joint Service Specification Guide, Aircraft Structures. Department of Defense: Washington, DC, USA, 1998.
3. NASA-HDBK-5010, Fracture Control Handbook for Payloads, Experiments, And Similar Hardware, May 2005, Revalidated 2012. Available online: https://standards.nasa.gov/standard/nasa/nasa-hdbk-5010 (accessed on 2 August 2021).
4. *EZ-SB-19-01*; Structures Bulletin. Durability and Damage Tolerance Certification for Additive Manufacturing of Aircraft Structural Metallic Parts. Wright Patterson Air Force Base: Dayton, OH, USA, 2019.
5. Lincoln, J.W.; Melliere, R.A. Economic life determination for a military aircraft. *J. Aircr.* **1999**, *36*, 737–742. [CrossRef]
6. Jones, R. Fatigue crack growth and damage tolerance. *Fatigue Fract. Eng. Mater. Struct.* **2014**, *37*, 463–483. [CrossRef]
7. Kundu, S.; Jones, R.; Peng, D.; Matthews, N.; Alankar, A.; Raman, S.R.; Huang, P. Review of requirements for the durability and damage tolerance certification of additively manufactured aircraft structural parts and AM repairs. *Materials* **2020**, *13*, 1341. [CrossRef] [PubMed]

8. Jones, R.; Peng, D. A building block approach to sustainment and durability assessment: Experiment and analysis. In *Comprehensive Structural Integrity*, 2nd ed.; Aliabadi, F.M.H., Soboyejo, W., Eds.; Elsevier: Oxford, UK, 2023; Volume 7, pp. 73–101. ISBN 978-0-12-822944-6.
9. *ASTM E647-13a*; Measurement of Fatigue Crack Growth Rates. ASTM: West Conshohocken, PA, USA, 2013.
10. Sanaei, N.; Fatemi, A. Defect-based fatigue life prediction of L-PBF additive manufactured metals. *Eng. Fract. Mech.* **2021**, *244*, 107541. [CrossRef]
11. Sanaei, N.; Fatemi, A. Defects in additive manufactured metals and their effect on fatigue performance: A state-of-the-art review. *Prog. Mater. Sci.* **2020**, *117*, 100724. [CrossRef]
12. Shamir, M.; Zhang, X.; Syed, A.K. Characterising and representing small crack growth in an additive manufactured titanium alloy. *Eng. Fract. Mech.* **2021**, *253*, 108876. [CrossRef]
13. Shamir, M.; Igwemezie, I.; Lotfian, S.; Jones, R.; Asif, H.; Ganguly, S.; Mehmanparast, A. Assessment of mechanical and fatigue crack growth properties of wire + arc additively manufactured mild steel components. *Fatigue Fract. Eng. Mater. Struct.* **2022**, *45*, 2978–2989. [CrossRef]
14. Dastgerdi, J.N.; Jaberi, O.; Remes, H.; Lehto, P.; Toudeshky, H.H.; Kuva, J. Fatigue damage process of additively manufactured 316L steel using X-ray computed tomography imaging. *Addit. Manuf.* **2023**, *70*, 103559. [CrossRef]
15. Peng, D.; Champagne, V.K.; Ang, A.S.M.; Birt, A.; Michelson, A.; Pinches, S.; Jones, R. Computing the Durability of WAAM 18Ni-250 Maraging Steel Specimens with Surface Breaking Porosity. *Crystals* **2023**, *13*, 443. [CrossRef]
16. Iliopoulos, A.P.; Jones, R.; Michopoulos, J.G.; Phan, N.; Raman, R.S. Crack growth in a range of additively manufactured aerospace structural materials. *Aerospace* **2018**, *5*, 118. [CrossRef]
17. Iliopoulos, A.P.; Jones, R.; Michopoulos, J.G.; Phan, N.; Rans, C. Further Studies into Crack Growth in Additively Manufactured Materials. *Materials* **2020**, *13*, 2223. [CrossRef] [PubMed]
18. Jones, R.; Rans, C.; Iliopoulos, A.P.; Michopoulos, J.G.; Phan, N.; Peng, D. Modelling the Variability and the Anisotropic Behaviour of Crack Growth in SLM Ti-6Al-4V. *Materials* **2021**, *14*, 1400. [CrossRef] [PubMed]
19. Jones, R.; Cizek, J.; Kovarik, O.; Lang, J.; Ang, A.; Michopoulos, J.G. Describing crack growth in additively manufactured Scalmalloy®. *Addit. Manuf. Lett.* **2021**, *1*, 100020. [CrossRef]
20. Jones, R.; Cizek, J.; Kovarik, O.; Ang, A.; Champagne, V. Observations on comparable aluminium alloy crack growth curves: Additively manufactured Scalmalloy® as an alternative to AA5754 and AA6061-T6 alloys? *Add. Manuf. Lett.* **2022**, *2*, 100026. [CrossRef]
21. Peng, D.; Jones, R.; Ang, A.S.M.; Michelson, A.; Champagne, V.; Birt, A.; Pinches, S.; Kundu, S.; Alankar, A.; Singh Raman, R.K. Computing the durability of WAAM 18Ni 250 Maraging steel specimens. *Fatigue Fract Eng. Mater Struct.* **2022**, *45*, 3535–3545. [CrossRef]
22. Jones, R.; Michopoulos, J.G.; Illiopoulos, A.P.; Raman, R.S.; Phan, N.; Nguyen, T. Representing crack growth in additively manufactured Ti-6Al-4V. *Int. J. Fatigue* **2018**, *116*, 610–622. [CrossRef]
23. Jones, R.; Molaei, R.; Fatemi, A.; Peng, D.; Phan, N. A note on computing the growth of small cracks in AM Ti-6Al-4V. *Procedia Struct. Integr.* **2020**, *28*, 364–369. [CrossRef]
24. Jones, R.; Kovarik, O.; Cizek, J.; Ang, A.; Lang, J. Crack growth in conventionally manufactured pure nickel, titanium and aluminium and the cold spray additively manufactured equivalents. *Addit. Manuf. Lett.* **2022**, *34*, 100043. [CrossRef]
25. Jones, R.; Kovarik, O.; Bagherifard, S.; Cizek, J.; Lang, J.; Papyan, V. Damage tolerance assessment of AM 304L and cold spray fabricated 316L steels and its implications for attritable aircraft. *Eng. Fract. Mech.* **2021**, *254*, 107916. [CrossRef]
26. Peng, D.; Tang, C.; Matthews, N.; Jones, R.; Kundu, S.; Singh Raman, R.K.; Alankar, A. Computing the Fatigue Life of Cold Spray Repairs to Simulated Corrosion Damage. *Materials* **2021**, *14*, 4451. [CrossRef]
27. Zhang, Y.; Zheng, K.; Heng, J.; Zhu, J. Corrosion-Fatigue Evaluation of Uncoated Weathering Steel Bridges. *Appl. Sci.* **2019**, *9*, 3461. [CrossRef]
28. Lo, M.; Jones, R.; Bowler, A.; Dorman, M.; Edwards, D. Crack growth at fastener holes containing intergranular cracking. *Fatigue Fract. Eng. Mater. Struct.* **2017**, *40*, 1664–1675. [CrossRef]
29. Tamboli, D.; Barter, S.; Jones, R. On the growth of cracks from etch pits and the scatter associated with them under a miniTWIST spectrum. *Int. J. Fatigue* **2018**, *109*, 10–16. [CrossRef]
30. Tan, J.L.; Chen, B.K. Prediction of fatigue life in aluminum alloy (AA7050-T7451) structures in the presence of multiple artificial short cracks. *Theor. Appl. Fract. Mech.* **2015**, *78*, 1–7. [CrossRef]
31. Main, B.; Evans, R.; Walker, K.; Yu, X.; Molent, L. Lessons from a fatigue prediction challenge for an aircraft wing shear tie post. *Int. J. Fatigue* **2019**, *123*, 53–65. [CrossRef]
32. Huang, P.; Yin, Y.; McNaulty, D.; Yan, W. A Damage Tolerance Approach for Structural Integrity of Truck Trailers. *Eng. Fail. Anal.* **2022**, *136*, 106197. [CrossRef]
33. Godefroid, L.B.; Moreira, L.P.; Vilela, T.C.G.; Faria, G.L.; Candido, L.C.; Pinto, E.S. Effect of chemical composition and microstructure on the fatigue crack growth resistance of pearlitic steels for railroad application. *Int. J. Fatigue* **2019**, *120*, 241–253. [CrossRef]
34. Clerc, G.; Brunner, A.J.; Niemz, P.; Van De Kuilen, J.W.G. Feasibility study on Hartman-Schijve data analysis for Mode II fatigue fracture of adhesively bonded wood joints. *Int. J. Fract.* **2019**, *221*, 123–140. [CrossRef]

35. Mael, A.; Eric, L.; Thomas, B.; Peter, D. Effect of aging on the fatigue crack growth properties of carbon-polyamide 6 thermoplastic composites using the multi ΔG-control method. *Compos. Part A Appl. Sci. Manuf.* **2022**, *161*, 107105. [CrossRef]
36. Rocha, A.V.M.; Akhavan-Safar, A.; Carbas, R.; Marques, E.A.S.; Goyal, R.; El-Zein, M.; da Silva, L.F.M. Paris law relations for an epoxy-based adhesive. *Proc. Inst. Mech. Eng. Part L J. Mater. Des. Appl.* **2019**, *234*, 291–299. [CrossRef]
37. Cano, A.; Salazar, A.; Rodríguez, J. Evaluation of different crack driving forces for describing the fatigue crack growth behaviour of PET-G. *Int. J. Fatigue* **2018**, *107*, 27–32. [CrossRef]
38. Kinloch, A.J.; Jones, R.; Michopoulos, J.G. Fatigue crack growth in epoxy polymer nanocomposites. *Philos. Trans. A R. Soc.* **2021**, *379*, 20200436. [CrossRef] [PubMed]
39. Simon, I.; Banks-Sills, L.; Fourman, V. Mode I delamination propagation and R-ratio e?ects in woven composite DCB specimens for a multi-directional layup. *Int. J. Fatigue* **2017**, *96*, 237–251. [CrossRef]
40. Banks-Sills, L.; Chocron, T.; Simon, I. Multi-directional composite laminates: Fatigue delamination propagation in mode I—A comparison. *Int. J. Fract.* **2019**, *219*, 175–185. [CrossRef]
41. Chocron, T.; Banks-Sills, L. Nearly mode I fracture toughness and fatigue delamination propagation in a multidirectional laminate fabricated by a wet-layup. *Phys. Mesomech.* **2019**, *22*, 107–140. [CrossRef]
42. Riedl, G.; Pugstaller, R.; Wallner, G.M. Development and implementation of a simultaneous fatigue crack growth test setup for polymeric hybrid laminates. *Eng. Fract. Mech.* **2022**, *267*, 108468. [CrossRef]
43. Brunner, A.J.; Stelzer, S.; Pinter, G.; Terrasi, G.P. Cyclic fatigue delamination of carbon fiber-reinforced polymer-matrix composites: Data analysis and design considerations. *Int. J. Fatigue* **2016**, *83*, 293–299. [CrossRef]
44. Jones, R.; Kinloch, A.J.; Michopoulos, J.G.; Brunner, A.J.; Phan, N. Delamination growth in polymer-matrix fibre composites and the use of fracture mechanics data for material characterisation and life prediction. *Compos. Struct.* **2017**, *180*, 316–333. [CrossRef]
45. Yao, L.; Alderliesten, R.; Jones, R.; Kinloch, A.J. Delamination fatigue growth in polymer-matrix fibre composites: A methodology for determining the design and lifing allowables. *Compos. Struct.* **2018**, *96*, 8–20. [CrossRef]
46. Jones, R.; Kinloch, A.J.; Michopoulos, J.; Iliopoulos, A.P. Crack growth in adhesives: Similitude and the Hartman-Schijve equation. *Compos. Struct.* **2021**, *273*, 114260. [CrossRef]
47. Kovarik, O.; Cizek, J.; Klecka, J. Fatigue Crack Growth Rate Description of RF-Plasma-Sprayed Refractory Metals and Alloys. *Materials* **2023**, *16*, 1713. [CrossRef] [PubMed]
48. Schwalbe, K.-H. On the beauty of analytical models for fatigue crack propagation and fracture-A personal historical review. *Fatigue Fract. Mech.* **2011**, *37*, 3–73. [CrossRef]
49. Rozumek, D. Survey of formulas used to describe the fatigue crack growth rate. *Mater. Sci.* **2014**, *49*, 723–733. [CrossRef]
50. Morgan, K.; Wells, D. Overview of Fatigue and Damage Tolerance Performance of SLM Alloy 718. In Proceedings of the 2016 National Space and Missile Materials Symposium, Westminster, CO, USA, 20–23 June 2016. Available online: https://ntrs.nasa.gov/archive/nasa/casi.ntrs.nasa.gov/20160007853.pdf (accessed on 1 June 2023).
51. Konečná, R.; Kunz, L.; Nicoletto, G.; Bača, A. Fatigue crack growth behavior of Inconel 718 produced by selective laser melting. *Frat. Ed Integrità Strutt.* **2016**, *35*, 31–40. [CrossRef]
52. Newman, J.C., Jr.; Yamada, Y. Compression Precracking Methods to Generate Near-Threshold Fatigue-Crack-Growth-Rate Data. *Int. J. Fatigue* **2010**, *32*, 879–885. [CrossRef]
53. Yadollahi, A.; Mahtabi, M.J.; Khalili, A.; Doude, H.R.; Newman, J.C., Jr. Fatigue life prediction of additively manufactured material: Effects of surface roughness, defect size, and shape. *Fatigue Fract. Eng. Mater. Struct.* **2018**, *41*, 1602–1614. [CrossRef]
54. Ostergaard, H.E.; Pribe, J.D.; Hasib, M.T.; Paradowska, A.M.; Siegmund, T.; Kruzic, J.J. Near-threshold fatigue crack growth in laser powder bed fusion produced alloy 718. *Int. J. Fatigue* **2022**, *163*, 107041. [CrossRef]
55. Kim, S.; Choi, H.; Lee, J.; Kim, S. Room and elevated temperature fatigue crack propagation behavior of Inconel 718 alloy fabricated by laser powder bed fusion. *Int. J. Fatigue* **2020**, *140*, 105802. [CrossRef]
56. Yu, X.; Lin, X.; Tan, H.; Hu, Y.; Zhang, S.; Liu, F.; Yang, H.; Huang, W. Microstructure and fatigue crack growth behavior of Inconel 718 superalloy fabricated via laser directed energy deposition additive manufacturing. *Int. J. Fatigue* **2021**, *143*, 106005. [CrossRef]
57. Paluskiewicz, S.A.; Narasimhachary, S.B.; Shinde, S.R.; Kain, C.; Towner, Z.B.; Muhlstein, C.L. Crack closure of Ni-based superalloy 718 at high negative stress ratios. *Int. J. Fatigue* **2022**, *160*, 106822. [CrossRef]
58. Iliopoulos, A.; Michopoulos, J.G.; Jones, R.; Kinloch, A.J.; Peng, D. A Framework for Automating the Parameter Determination of Crack Growth Models. *Int. J. Fatigue* **2023**, *169*, 107490. [CrossRef]
59. Poulin, J.-R.; Brailovski, V.; Terriault, P. Long fatigue crack propagation behavior of Inconel 625 processed by laser powder bed fusion: Influence of build orientation and post-processing conditions. *Int. J. Fatigue* **2018**, *116*, 634–647. [CrossRef]
60. Poulin, J.-R.; Kreitcberg, A.; Brailovski, V. Effect of Hot Isostatic Pressing of laser powder bed fused Inconel 625 with purposely induced defects on the residual porosity and fatigue crack propagation behaviour. *Addit. Manuf.* **2021**, *47*, 102324. [CrossRef]
61. Poulin, J.-R.; Kreitcberg, A.; Terriault, P. Long fatigue crack propagation behavior of laser powder bed-fused Inconel 625 with intentionally-seeded porosity. *Int. J. Fatigue* **2019**, *127*, 144–156. [CrossRef]

62. Hu, X.; Xue, Z.; Ren, T.; Jiang, Y.; Dong, C.; Liu, F. On the fatigue crack growth behaviour of selective laser melting fabricated Inconel 625: Effects of build orientation and stress ratio. *Fatigue Fract. Eng. Mater. Struct.* **2020**, *43*, 771–787. [CrossRef]
63. Jones, R.; Singh Raman, R.K.; McMillan, A.J. Crack growth: Does microstructure play a role? *Eng. Fract. Mech.* **2018**, *187*, 190–210. [CrossRef]